COMPDYN 2015
5th ECCOMAS Thematic Conference on
Computational Methods in Structural Dynamics and Earthquake Engineering
M. Papadrakakis, V. Papadopoulos, V. Plevris (eds.)
Crete Island, Greece, 25–27 May 2015

EXPERIMENTAL AND NUMERICAL EVALUATION OF THE EFFICIENCY OF A STIFF WAVE BARRIER IN THE SOIL

Pieter Coulier[1], Vicente Cuéllar[2], Geert Degrande[1], and Geert Lombaert[1]

[1]KU Leuven, Department of Civil Engineering
Kasteelpark Arenberg 40, 3001 Leuven, Belgium
e-mail: {pieter.coulier,geert.degrande,geert.lombaert}@bwk.kuleuven.be

[2]CEDEX, Laboratoria de Geotecnia
Alfonso XII 3, 28014 Madrid, Spain
e-mail: vicente.cuellar@cedex.es

Keywords: Railway induced vibrations, stiff wave barrier, in situ experiment, vibration mitigation.

Abstract. *This paper discusses the design, the installation, and the experimental and numerical evaluation of the effectiveness of a stiff wave barrier in the soil as a mitigation measure for railway induced vibrations. A full scale in situ experiment has been conducted at a site in El Realengo (Spain), where a barrier consisting of overlapping jet grout columns has been installed along a railway track. This barrier is stiff compared to the soil and has a depth of* $7.5\,\mathrm{m}$*, a width of* $1\,\mathrm{m}$*, and a length of* $55\,\mathrm{m}$*. Geophysical tests have been performed prior to the installation of the barrier for the determination of the dynamic soil characteristics. Extensive measurements have been carried out before and after installation of the barrier; this paper focuses on free field vibrations during train passages. Measurements have also been performed at a reference section adjacent to the test section in order to verify the effect of changing train, track, and soil conditions over time. The in situ measurements show that the barrier is very effective: during train passages, a reduction of vibration levels by* $5\,\mathrm{dB}$ *is already obtained from* $8\,\mathrm{Hz}$ *upwards, while a peak reduction of about* $12\,\mathrm{dB}$ *is observed near* $30\,\mathrm{Hz}$ *immediately behind the barrier. The performance decreases further away from the jet grouting wall, but remains significant. This in situ test hence serves as a 'proof of concept', demonstrating that stiff wave barriers are capable of significantly reducing vibration levels, provided that they are properly designed.*

1 INTRODUCTION

Railway induced vibrations can lead to annoyance for residents of nearby buildings. During the past decades, a lot of research has been performed to develop efficient and cost–effective vibration countermeasures for reducing excessive levels of building vibration [1, 2, 3]. Measures can either be taken at the source (railway track) [4, 5, 6], on the propagation path between source and receiver [7, 8, 9], or at the receiver (building) [10, 11]. An advantage of interventions on the propagation path is that no modifications to the track are required, while multiple buildings can be protected simultaneously from vibration. Furthermore, this type of measures can relatively easily be implemented along an existing track.

A basic type of a mitigation measure on the propagation path is an open trench in the soil. The latter aims at reflecting the impinging waves and is expected to be effective if its depth is comparable to the penetration depth of the Rayleigh waves in the soil. The effectiveness of open trenches has been investigated numerically by many authors as Woods [12], Segol et al. [13], Beskos et al. [14], and Klein et al. [15]. For stability reasons, the construction of an open trench in the soil is limited to shallow depths. Furthermore, an open trench can easily get inundated due to surface water run–off or groundwater infiltration, posing concerns on effectiveness, durability, and safety. The use of either soft (polystyrene [9], rubber chips [16]) or stiff (concrete, grout) in–fill materials (compared to the original soil) allows reaching larger depths and results in a more sustainable solution. Various numerical approaches have been explored for predicting the effectiveness of open and in–filled trenches, such as the finite element (FE) [17], the boundary element (BE) [18], or coupled FE–BE methods [9]. Other examples of vibration mitigation measures on the propagation path include buried wall barriers [19], wave impeding blocks [20], rows of piles [21], and heavy masses placed along a railway track for scattering the incident surface waves [22, 23].

Although numerical simulations are indispensable for understanding and designing efficient wave barriers, there remains a strong need to validate the outcome of these simulations by means of in situ tests. Early experiments with trenches have been reported by Woods [12], while results from more recent field measurements involving open and filled trenches have been presented by Al–Hussaini et al. [24] and Çelebi et al. [25]. The use of a soft geofoam in–fill material has been assessed experimentally by Alzawi and El Naggar [17]; François et al. [9] describe the design and efficiency of a composite vibration isolation screen near a tramway in Brussels. In most of the aforementioned experiments, the length of the vibration isolation screens was limited to a few meters and only artificial excitation sources such as impact hammers or harmonic shakers were employed for assessing the isolation performance. Examples of longer screens (tens of meters) can be found in Sweden and Germany, where gas–filled cushions have been installed and tested [26, 27]. Apart from in situ experiments, complementary small scale laboratory tests are also valuable. Haupt [28] presents model tests of various types of barriers, while Murillo et al. [29] have investigated the efficiency of expanded polystyrene (EPS) barriers by means of centrifuge tests. A small scale experimental study of a stiff wave barrier in gelatine has been reported in [30].

This paper presents a full scale in situ experiment that has been specifically designed for assessing the performance of stiff wave barriers in the soil. The circumstances in which such barriers are expected to be effective have been analysed in detail in [31] by means of state–of–the–art numerical simulations, highlighting how their performance critically depends on site specific characteristics such as dynamic soil properties. Furthermore, the physical mechanism that results in a reduction of vibration levels for stiff barriers has been identified and was found

to fundamentally differ from that of open trenches or soft barriers. Based on these findings, a field test has been designed and carried out in Spain within the frame of the EU FP7 project RIVAS (Railway Induced Vibration Abatement Solutions) [32], which forms the topic of the present paper. A more elaborate discussion with additional experimental results as well as a comparison with numerical simulations can be found in [33].

The outline of this paper is as follows. Section 2 introduces the test site in Spain and addresses the determination of the dynamic soil characteristics. The design and construction of the stiff wave barrier are also discussed, while the main physical principles affecting the performance of this type of barrier are briefly reviewed. The measured free field response during train passages before and after installation of the barrier is subsequently presented in section 3. Conclusions are drawn in section 4.

2 EXPERIMENTAL SETUP

2.1 Description of the test site

A suitable site for testing a stiff wave barrier was identified in El Realengo (south–east of Spain) along the conventional railway line between Murcia and Alicante. The track at this site is a classical ballasted track with bi–block reinforced concrete sleepers supporting RN 45 rails with Spanish wide gauge ($1.668\,\mathrm{m}$). It is supported by a ballast layer and an embankment, each $0.50\,\mathrm{m}$ high. Geotechnical studies, performed in preparation of the construction of a new high speed railway line next to the conventional line, indicated the presence of soft silty clay soil layers with a thickness of approximately $10\,\mathrm{m}$ on top of stiffer alluvial soil. These are particular circumstances where a stiff wave barrier is expected to be very effective [31]. At the site, a test section as well as a reference section were chosen, as indicated on figure 1. The jet grouting wall is implemented along the test section; the aim of the reference section is to verify the effect of changing track, train, and soil conditions over time. This is important when evaluating the mitigation performance of the wave barrier, as will be discussed in detail in section 3.

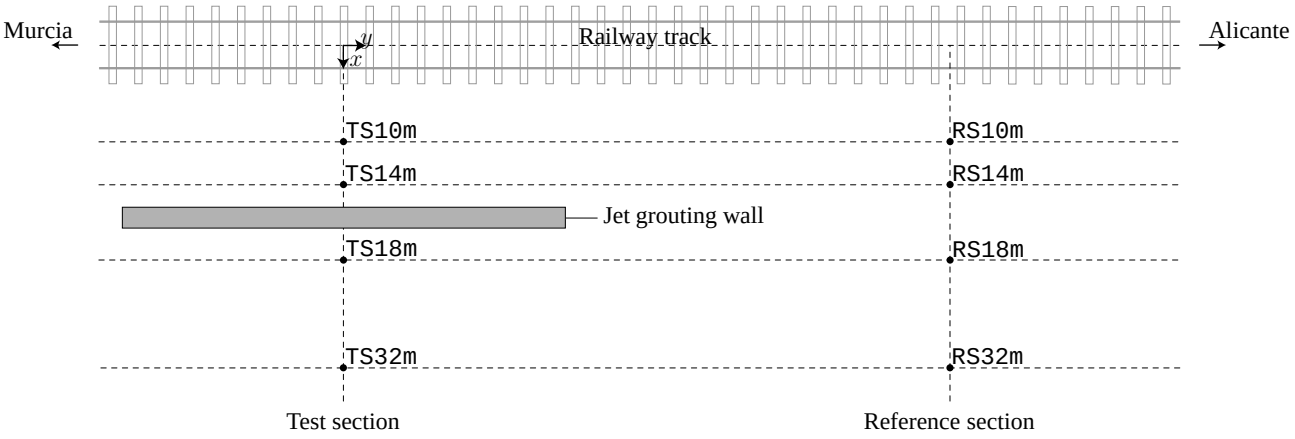

Figure 1: Setup for the measurement of the free field response due to train passages (figure not to scale).

2.2 Determination of the dynamic soil characteristics

As numerical simulations indicate that the vibration mitigation efficiency of a stiff wave barrier strongly depends on the dynamic soil characteristics [31], several geotechnical and geophysical tests were carried out for an accurate determination of these properties. This includes Spec-

tral Analysis of Surface Waves (SASW) tests, seismic piezocone down–hole tests (SCPTU), and seismic refraction tests. These tests have allowed for the identification of a simplified horizontally layered soil model, as summarized in table 1 (layer thickness h, shear wave velocity C_s, dilatational wave velocity C_p, material damping ratios β_s and β_p in both deviatoric and volumetric deformation, density ρ). The soil densities given in the table are those determined from undisturbed samples retrieved from boreholes drilled in preparation of the construction of the new high speed railway line. The identified soil profile confirms the presence of a soft layer of silty clay with a thickness of approximately $10\,\mathrm{m}$ (layers 2 and 3) that overlies hard alluvial soil. The soil is saturated at depths below $1.50\,\mathrm{m}$ due to the presence of the ground water table. This leads to a high dilatational wave velocity C_p for layers 3, 4, and 5.

Layer	h [m]	C_s [m/s]	C_p [m/s]	β_s [-]	β_p [-]	ρ [kg/m^3]
1	0.30	270	560	0.123	0.123	1800
2	1.20	150	470	0.112	0.112	1750
3	8.50	150	1560	0.014	0.014	1750
4	10.00	475	1560	0.010	0.010	1900
5	∞	550	2030	0.010	0.010	1900

Table 1: Dynamic soil characteristics at the site in El Realengo.

The dynamic soil characteristics summarized in table 1 have subsequently been used to calculate free field transfer functions. Figure 2 shows the transfer functions between a vertical point source and the vertical velocity at $8\,\mathrm{m}$ and $16\,\mathrm{m}$ from the source. With increasing distance from the source, the transfer functions show a stronger decrease at higher frequencies due to material damping in the soil. The predictions are compared to the mean value and the 95% confidence interval of the measured transfer functions at the test and reference section. The latter have been determined using the H_1–estimator, which is based on the average cross and auto power spectral densities [34]. A good agreement is found between the predictions and the experimental results, in particular in the frequency range up to $50\,\mathrm{Hz}$. This demonstrates that the dynamic soil properties have been identified with sufficient accuracy for making reliable numerical predictions. The signal–to–noise ratio decreases at higher frequencies which leads to a large confidence interval, however, making it more difficult to assess the accuracy of the predictions. Furthermore, figure 2 shows a significant difference between the transfer functions measured at the test and reference section, hence indicating a spatial variability of the dynamic soil characteristics.

2.3 Design of the stiff wave barrier

Numerical simulations have revealed that a stiff wave barrier in the soil can be a very effective vibration countermeasure, which is due to the interaction between Rayleigh waves in the soil and bending waves in the barrier [31, 35]. The mechanism that leads to a reduction of free field vibrations is concisely summarized in the following paragraphs; the reader is referred to [31, 35] for a detailed discussion.

Figure 3a shows the real part of the vertical displacement $u_z(\mathbf{x}, f)$ in the soil due to a unit harmonic point load at $5\,\mathrm{Hz}$ and $15\,\mathrm{Hz}$ at the surface of the halfspace, if no barrier is present. The railway track is disregarded in order to facilitate physical interpretation. The propagation of Rayleigh waves can clearly be observed. The wavefield in the case of an infinitely long stiff

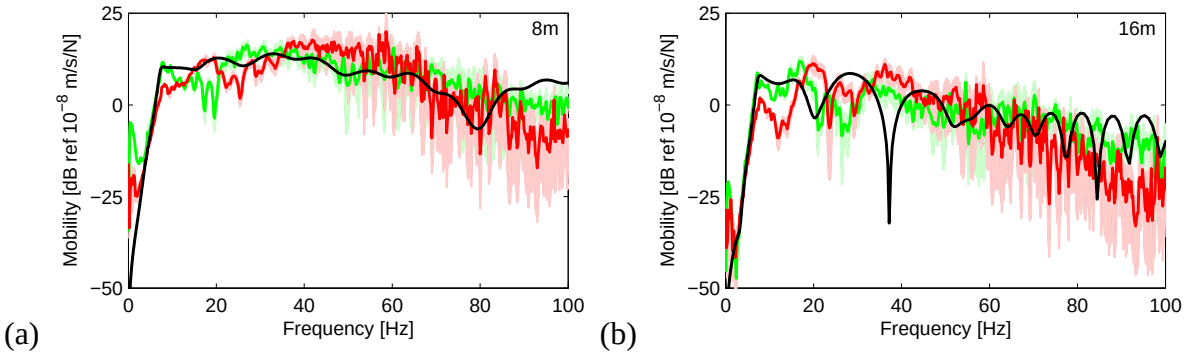

Figure 2: Predicted free field transfer functions (black line) compared to the experimental results at the test (red line) and reference (green line) section at (a) $8\,\mathrm{m}$ and (b) $16\,\mathrm{m}$ from the impact point. The 95% confidence interval of the measurements is indicated as a shaded area.

barrier (with a depth of $7.5\,\mathrm{m}$, a width of $1\,\mathrm{m}$, and dynamic characteristics as listed in table 2) embedded in the soil is shown in figure 3b. The barrier's vibration reduction effectiveness is quantified through the vertical insertion loss $\mathrm{IL}_z(\mathbf{x}, f) = 20\log_{10}\left(|u_z^{\mathrm{ref}}(\mathbf{x}, f)|/|u_z(\mathbf{x}, f)|\right)$ in figure 3c, where positive values of the insertion loss indicate a reduction of the vertical free field vibrations. Figure 3c indicates that the barrier is unable to impede the propagation of Rayleigh waves at $5\,\mathrm{Hz}$, while a significant reduction of vibration levels is achieved at $15\,\mathrm{Hz}$, but only in a limited area behind the barrier.

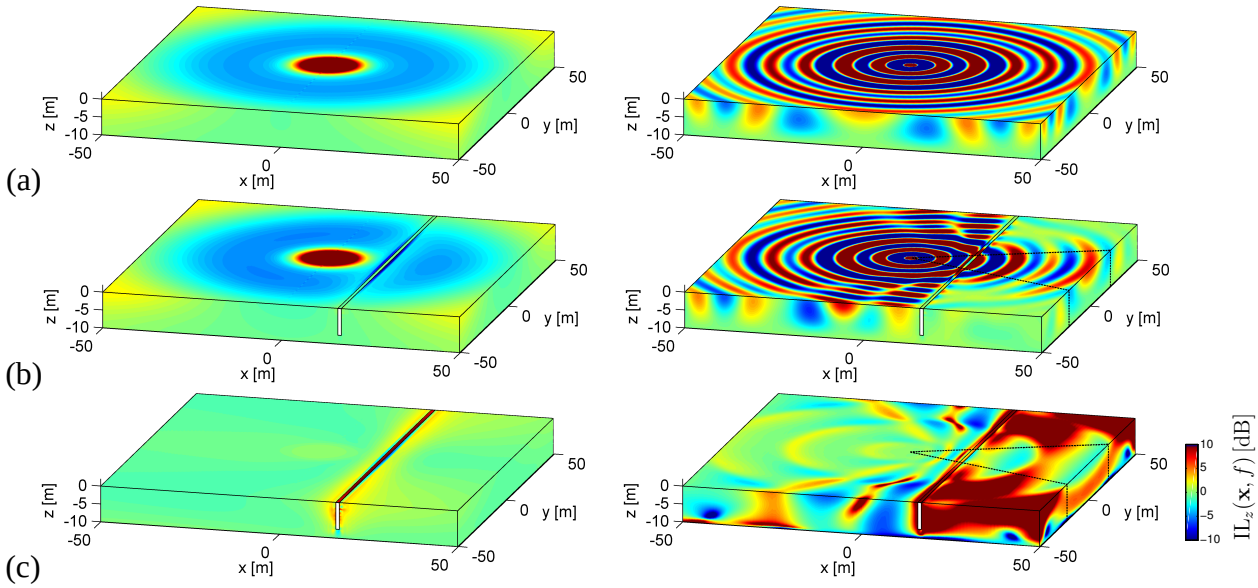

Figure 3: Real part of the vertical displacement $u_z(\mathbf{x}, f)$ due to harmonic excitation at $5\,\mathrm{Hz}$ (left hand side) and $15\,\mathrm{Hz}$ (right hand side) (a) without and (b) with a stiff wave barrier. The corresponding insertion loss $\mathrm{IL}_z(\mathbf{x}, f)$ is shown in (c). The dotted lines in (b) and (c) delimit $2\theta_{\mathrm{c}}(f)$.

The observations in figure 3 can be explained by considering a decomposition of the wavefield into plane waves, satisfying the Rayleigh wave dispersion relation $1/\lambda_x^2 + 1/\lambda_y^2 = 1/\lambda_{\mathrm{R}}^2(f)$ [36]. For propagating plane waves, the trace wavelength λ_y observed by the barrier is situated between $\lambda_y = \infty$ (for plane waves impinging perpendicularly on the barrier) and $\lambda_y = \lambda_{\mathrm{R}}(f) = C_{\mathrm{R}}(f)/f$ (for plane waves travelling along the barrier), where $C_{\mathrm{R}}(f)$ is the frequency depen-

dent velocity of the fundamental Rayleigh wave in the soil. Figure 4 compares $C_{\mathrm{R}}(f)$ to the velocity of a free bending wave in the stiff wave barrier $C_{\mathrm{b}}(f)$. The latter is obtained using Timoshenko beam theory and assuming bending with respect to the barrier's horizontal axis. At low frequencies (i.e. $5\,\mathrm{Hz}$ in figure 3), the Rayleigh wave velocity $C_{\mathrm{R}}(f)$ is larger than the bending wave velocity $C_{\mathrm{b}}(f)$ and all plane waves in the soil have a trace wavelength λ_y larger than the free bending wavelength $\lambda_{\mathrm{b}}(f) = C_{\mathrm{b}}(f)/f$ of the barrier ($\lambda_{\mathrm{b}}(f) < \lambda_{\mathrm{R}}(f) \leq \lambda_y \leq \infty$). These waves propagate unhindered through the barrier, as observed in figure 3. If the velocity $C_{\mathrm{R}}(f)$ matches the velocity $C_{\mathrm{b}}(f)$, a critical frequency f_{c} is attained. From this critical frequency $f_{\mathrm{c}} = 6.5\,\mathrm{Hz}$ upwards, the wavefield contains plane waves in the soil with a trace wavelength λ_y that is smaller than the free bending wavelength $\lambda_{\mathrm{b}}(f)$. The transmission of these plane waves is impeded by the stiff barrier, as the latter's bending stiffness varies proportionally to $(\lambda_{\mathrm{b}}/\lambda_y)^4$ at a given frequency. Waves with a trace wavelength λ_y larger than $\lambda_{\mathrm{b}}(f)$ remain unaffected by the presence of the barrier, however. As a result, a reduction of vibration levels is only achieved in an area delimited by a critical angle $\theta_{\mathrm{c}}(f) = \sin^{-1}\left(C_{\mathrm{R}}(f)/C_{\mathrm{b}}(f)\right)$, which can clearly be distinguished at $15\,\mathrm{Hz}$ on figure 3.

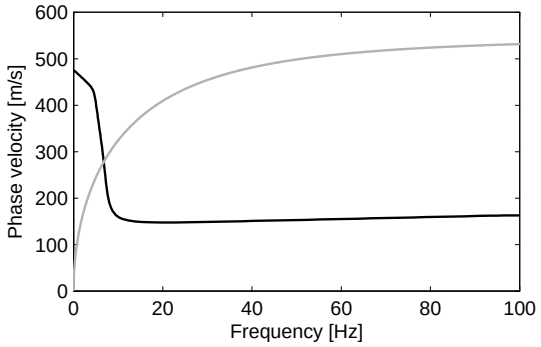

Figure 4: Phase velocity $C_{\mathrm{R}}(f)$ of the fundamental Rayleigh wave in the soil (black line) compared to the phase velocity $C_{\mathrm{b}}(f)$ of bending waves in the stiff barrier (grey line)

If the passage of a train is considered (rather than transfer functions as in figure 3), several dynamic axle loads contribute to the ground vibration at a certain receiver point of interest in the free field. Due to the existence of the critical angle $\theta_{\mathrm{c}}(f)$, the contribution of the axle loads moving towards or away from the receiver will be reduced more effectively than the contribution of the axle loads located near the receiver. The largest reduction is therefore expected to take place at locations close to the track (as the contribution of a larger number of axle loads is mitigated) and, at a particular location, at high frequencies (due to the decreasing critical angle).

2.4 Installation of the jet grouting wall

Several construction techniques are available for creating a stiff wave barrier in the soil, such as deep vibro–compaction, the installation of gravel or cement columns, hydraulic fracture injection with stable cement–bentonite mixtures, and vacuum consolidation. Jet grouting was selected as an appropriate technique for the site in El Realengo due to its versatility and possibility to strengthen a wide range of weak natural soils. Jet grouting is a bottom–up procedure, where grout is injected under high pressure at the design depth in order to initiate the erosion of the soil. A uniform rotation and lifting of the nozzle hence allows for the creation of in situ cemented column formations, while the spoil material is expelled at the top of the borehole. 60

overlapping grout columns with a diameter of $1.5\,\mathrm{m}$ and a centre–to–centre distance of $0.9\,\mathrm{m}$ were installed to create a stiff wave barrier with an overall length of $55\,\mathrm{m}$ and a width of $1\,\mathrm{m}$. This was achieved using a monofluid consisting of $90\,\mathrm{kg}$ of cement per $100\,\mathrm{l}$ of water injected under a pressure of $40,000\,\mathrm{kN/m^2}$, while maintaining a flow rate of $310 - 320\,\mathrm{l/min}$, a nozzle lift speed of $200\,\mathrm{mm/min}$, and a nozzle rotation speed of $20\,\mathrm{rpm}$ during the whole injection procedure. Figure 5a shows the equipment that has been employed for creating the jet grout columns, while the surface of the resulting wave barrier is shown in figure 5b. For safety reasons and due to the presence of a water duct, the barrier could only be constructed at a distance of $16.2\,\mathrm{m}$ from the center of the railway track.

(a)  (b) 

Figure 5: (a) Construction of the jet grout columns and (b) the stiff wave barrier upon completion at the site of El Realengo.

Five test columns were realized prior to the construction of the jet grouting wall. Furthermore, multiple test samples have been taken during the installation of the individual columns to verify their strength and stiffness. Laboratory tests (unconfined compression tests, non–dispersive P—S sonic tests, dispersive bender element tests) have been performed on these samples; the best estimate of the dynamic characteristics (two months after construction) is given in table 2. The lower part of the barrier is saturated, resulting in a higher dilatational wave velocity C_p and density ρ below a depth of $1.50\,\mathrm{m}$.

Layer	h [m]	C_s [m/s]	C_p [m/s]	β_s [-]	β_p [-]	ρ [kg/m^3]
1	1.50	600	1150	0.03*	0.03*	1400
2	6.00	600	1650	0.03*	0.03*	1750

Table 2: Dynamic characteristics of the jet grouting wall. Estimated values are indicated by a star.

3 EXPERIMENTAL EVALUATION OF THE VIBRATION MITIGATION PERFORMANCE

Extensive measurement campaigns have been carried out before and after installation of the stiff wave barrier in El Realengo in order to evaluate its performance. This includes the

measurement of the free field response due to train passages, transfer functions between the track and the free field, and track receptance tests. The experimental results are discussed in the following. Only train passages are discussed in this paper, however; the reader is referred to [33] for a discussion of the additional tests.

Passages of three different train types were recorded at the El Realengo site, before (October 2013) and after (December 2013) construction of the jet grouting wall: S592 commuter trains, S599 medium distance trains, and long distance Talgo VI trains. These are train passages on the classical ballasted track; the new high speed railway line was not in operation yet at the time of the experimental campaigns. In this paper, only results obtained during the passage of S592 commuter trains are discussed, as similar trends are found for the other train types. The S592 commuter train is a short train consisting of three carriages. Each carriage has two bogies, while each bogie is supported by two axles. The train has a total length of $65\,\mathrm{m}$ between the first and last axle. Each axle has an estimated unsprung mass of $2000\,\mathrm{kg}$. As only a single track is present at the site, both train passages from Murcia to Alicante and vice versa are recorded. The train velocities are estimated from strain measurements on the rails at the reference and test section. Ten and eleven passages of S592 trains have been recorded in October and December 2013, respectively, with a train speed varying between $112\,\mathrm{km/h}$ and $122\,\mathrm{km/h}$ (with an average speed of $117\,\mathrm{km/h}$). Free field vertical vibration velocities were measured by means of geophones along a line perpendicular to the track, at $10\,\mathrm{m}$, $14\,\mathrm{m}$, $18\,\mathrm{m}$, and $32\,\mathrm{m}$ from the outer rail, both at the reference and test section (and thus at $10.834\,\mathrm{m}$, $14.834\,\mathrm{m}$, $18.834\,\mathrm{m}$, and $32.834\,\mathrm{m}$ from the center of the track). These locations are referred to as RSxx and TSxx in the following, respectively, where the label xx represents the distance from the outer rail. The receiver locations at $18\,\mathrm{m}$ and $32\,\mathrm{m}$ at the test section are situated behind the jet grouting wall, as indicated on figure 1. Only vertical vibration velocities were recorded in this test, although vibrations in the transversal and longitudinal direction might also be of interest in practical situations [37].

Figure 6 shows the time history and frequency content of the vertical rail velocity at the test and reference section during the passage of a S592 commuter train at a speed of $117\,\mathrm{km/h}$ in December 2013, i.e. after construction of the jet grouting wall. This particular train runs from Murcia to Alicante, implying that it first passes the test section and subsequently the reference section, as can be observed in figure 6. The passage of each individual axle is clearly apparent in the time history, while the quasi–discrete spectrum is mainly situated below $20\,\mathrm{Hz}$. The response at the reference and test section are very similar, indicating that the track conditions at the reference and test section are alike, but also that the presence of the jet grouting wall has little effect on the response of the rail (as expected from numerical simulations [31]).

Figure 7 shows the time history and frequency content of the vertical free field velocity at the reference and test section during the same train passage. As the train approaches, the measured ground velocity increases, is subsequently followed by a nearly stationary part during the passage, and finally decreases when the train moves away. The passage of individual axles can no longer be distinguished as in the case of the rail response, however. The vibration amplitude decreases with increasing distance from the track; the high frequency components are especially attenuated due to material damping in the soil. Peaks are observed in the frequency spectrum near $10\,\mathrm{Hz}$ and $30\,\mathrm{Hz}$. Figures 7a and 7b indicate that the response at $10\,\mathrm{m}$ and $14\,\mathrm{m}$ from the track is slightly larger at the test section than at the reference section. As can be observed in figures 7c and 7d, the vibration levels at $18\,\mathrm{m}$ and $32\,\mathrm{m}$ from the track (i.e. behind the barrier) are significantly lower at the test section than at the reference section, especially from $8\,\mathrm{Hz}$ upwards. This clearly suggests that the jet grouting wall is effectively reducing the vibration levels.

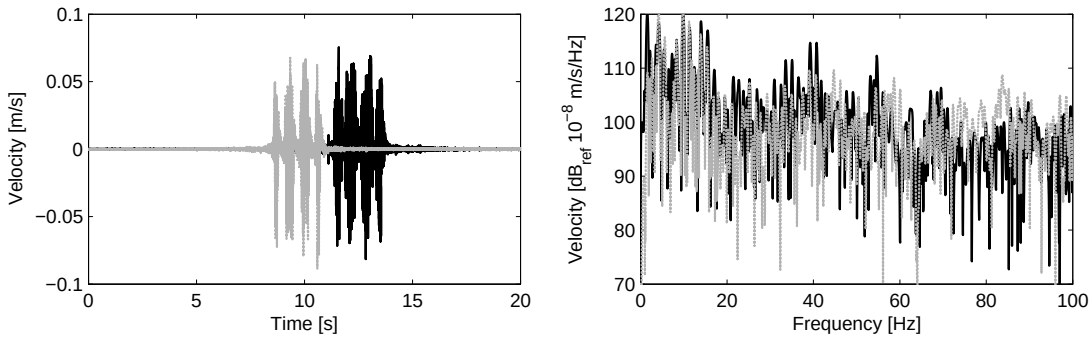

Figure 6: Time history (left) and frequency content (right) of the measured vertical rail velocity during the passage of a S592 commuter train at a speed of $117\,\mathrm{km/h}$ at the reference (solid black line) and test (dotted grey line) section.

Vibrations due to train passages can also be quantified in terms of the vibration velocity level $L_{\mathrm{v}}(f)$, which is defined as the one–third octave band spectrum of the stationary part of the vibration velocity $v_{z\mathrm{RMS}}(f)$:

$$L_{\mathrm{v}}(f) = 20\log_{10}\left(\frac{v_{z\mathrm{RMS}}(f)}{v_0}\right) \tag{1}$$

where $v_{z\mathrm{RMS}}(f)$ is the running Root Mean Square (RMS) value of the velocity, while $v_0 = 10^{-8}\,\mathrm{m/s}$ represents a reference velocity. The stationary part of the measured response during a train passage is selected using the German DIN standard [38]. Figure 8 shows the measured vibration velocity levels $L_{\mathrm{v}}(f)$ during the passages of all S592 commuter trains before and after construction of the jet grouting wall at the reference and test section, respectively. The arithmetically averaged vibration velocity levels $\bar{L}_{\mathrm{v}}(f)$ are also superimposed on figure 8. Although train passages of the same train type at approximately the same speed are considered, a considerable variation is observed in the frequency spectrum. This variability is caused by differences in train properties (train speed, wheel unevenness) and the variation of track characteristics (rail unevenness, ballast stiffness) and soil conditions (water table) in space and time. It is crucial to take the latter into account when evaluating the performance of the jet grouting wall. Despite the large variability between different train passages, it is nevertheless clear from figures 8c and 8d that the installation of the barrier leads to a significant reduction of vibration levels at the test section.

The vibration reduction effectiveness of the jet grouting wall is quantified by means of the vertical insertion loss $\mathrm{IL}_z(f)$. A first straightforward approach for determining $\mathrm{IL}_z(f)$ consists of comparing vibration velocity levels at the test section before and after installation of the barrier:

$$\mathrm{IL}_z(f) = L_{\mathrm{v}}^{\mathrm{test,before}}(f) - L_{\mathrm{v}}^{\mathrm{test,after}}(f) \tag{2}$$

This approach does not account for the changing train, track, and soil conditions in time, however, which might be significant as there was a two month period between the measurements before and after installation of the barrier. Alternatively, the insertion loss is computed by comparing vibration velocity levels at the reference and test section at the same moment (i.e. after installation of the barrier):

$$\mathrm{IL}_z(f) = L_{\mathrm{v}}^{\mathrm{ref,after}}(f) - L_{\mathrm{v}}^{\mathrm{test,after}}(f) \tag{3}$$

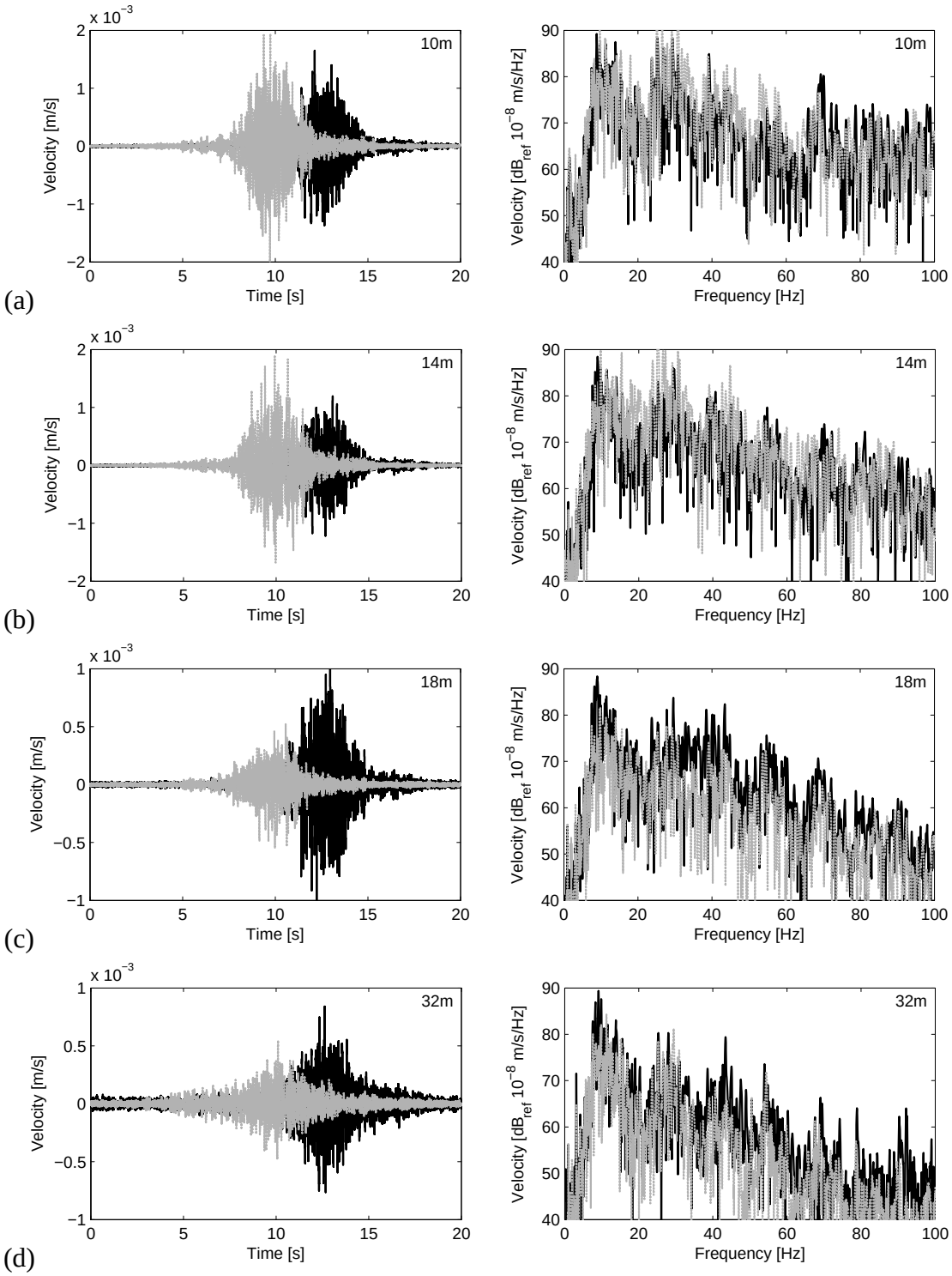

Figure 7: Time history (left) and frequency content (right) of the measured vertical free field vibration during the passage of a S592 commuter train at a speed of $117\,\mathrm{km/h}$ at the reference (solid black line) and test (dotted grey line) section, at (a) $10\,\mathrm{m}$, (b) $14\,\mathrm{m}$, (c) $18\,\mathrm{m}$, and (d) $32\,\mathrm{m}$ from the outer rail.

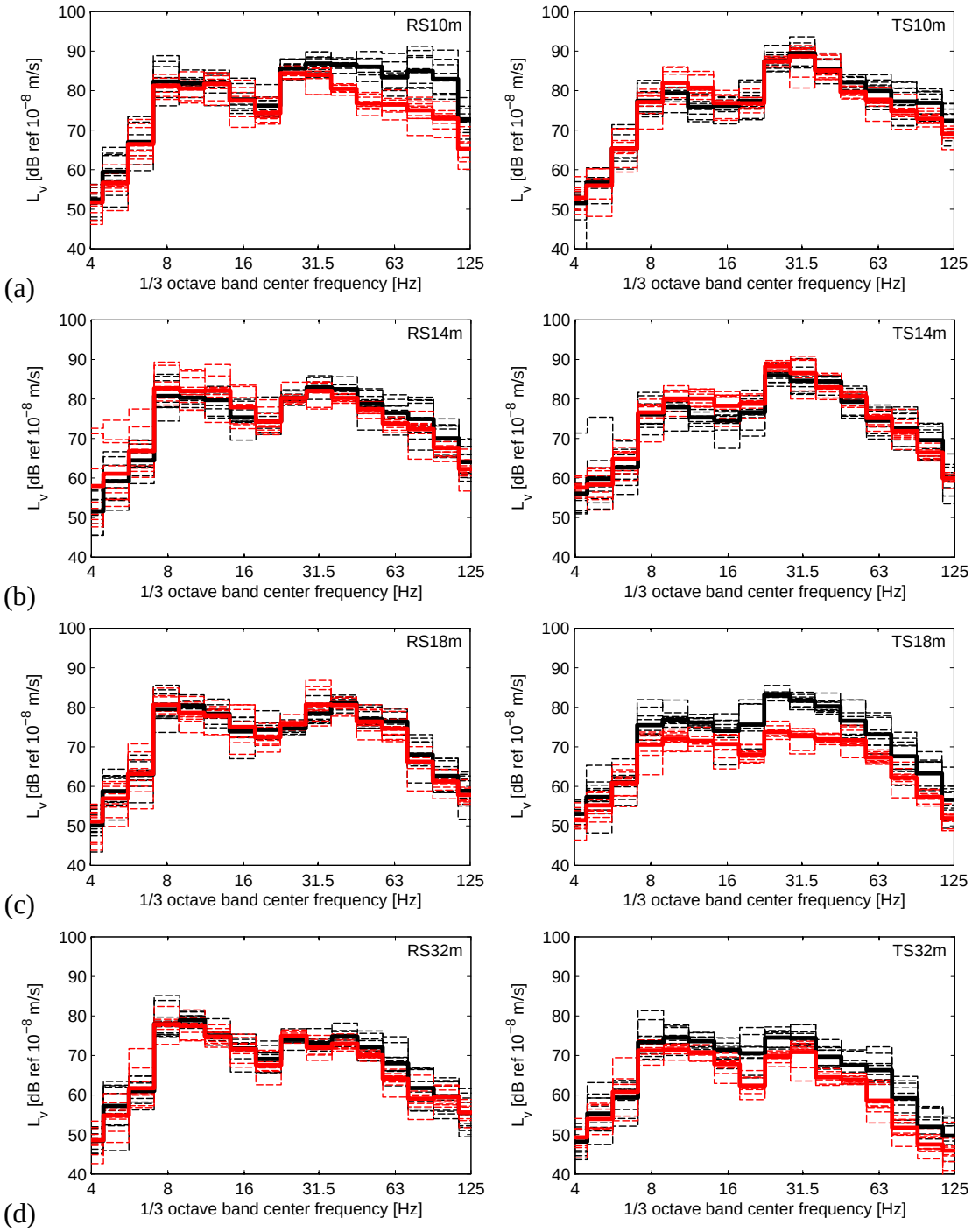

Figure 8: Measured vibration velocity levels $L_{\mathrm{v}}(f)$ in one–third octave bands at the reference (left) and test (right) section during the passage of S592 commuter trains before (dashed black lines) and after (dashed red lines) construction of the jet grouting wall, at (a) $10\,\mathrm{m}$, (b) $14\,\mathrm{m}$, (c) $18\,\mathrm{m}$, and (d) $32\,\mathrm{m}$ from the outer rail. The averaged vibration velocity levels $\bar{L}_{\mathrm{v}}(f)$ are indicated in solid bold lines.

The track and soil conditions at the reference and test section are not exactly the same, however, hampering the use of equation (3). A more rigorous quantification of the vibration mitigation performance is obtained in a combined procedure, in which measurements at the reference and test section before and after installation of the barrier are simultaneously accounted for [39]:

$$\begin{aligned} \mathrm{IL}_z(f) &= \left(L_\mathrm{v}^{\mathrm{test,before}}(f) - L_\mathrm{v}^{\mathrm{test,after}}(f)\right) - \left(L_\mathrm{v}^{\mathrm{ref,before}}(f) - L_\mathrm{v}^{\mathrm{ref,after}}(f)\right) && (4)\\ &= \Delta L_\mathrm{v}^{\mathrm{test}}(f) - \Delta L_\mathrm{v}^{\mathrm{ref}}(f) \\ &= \left(L_\mathrm{v}^{\mathrm{ref,after}}(f) - L_\mathrm{v}^{\mathrm{test,after}}(f)\right) - \left(L_\mathrm{v}^{\mathrm{ref,before}}(f) - L_\mathrm{v}^{\mathrm{test,before}}(f)\right) && (5)\\ &= \Delta L_\mathrm{v}^{\mathrm{after}}(f) - \Delta L_\mathrm{v}^{\mathrm{before}}(f) \end{aligned}$$

The first bracketed term $\Delta L_\mathrm{v}^{\mathrm{test}}(f)$ in equation (4) corresponds to equation (2) and characterizes the reduction of vibration levels at the test section, while the second term $\Delta L_\mathrm{v}^{\mathrm{ref}}(f)$ is a correction for possible variations in time, based on measurements at the reference section. The insertion loss is alternatively rewritten as equation (5), where the vibration levels at the reference and test section are compared as in equation (3), with a correction $\Delta L_\mathrm{v}^{\mathrm{before}}(f)$ for possible spatial variations between the reference and test section. Both expressions yield the same result, but equation (5) is particularly useful for assessing the variability of the insertion loss $\mathrm{IL}_z(f)$. The quantities $\Delta L_\mathrm{v}^{\mathrm{after}}(f)$ and $\Delta L_\mathrm{v}^{\mathrm{before}}(f)$ can be evaluated for each individual train passage before and after installation of the barrier, respectively, and their sample mean and variance can be computed straightforwardly. This allows estimating the sample variance of the insertion loss $\mathrm{IL}_z(f)$ as $\sigma^2_{\mathrm{IL}_z}(f) = \sigma^2_{\Delta L_\mathrm{v}^{\mathrm{after}}}(f) + \sigma^2_{\Delta L_\mathrm{v}^{\mathrm{before}}}(f)$, assuming that $\Delta L_\mathrm{v}^{\mathrm{after}}(f)$ and $\Delta L_\mathrm{v}^{\mathrm{before}}(f)$ are uncorrelated. This is not the case when employing equation (4), as the quantities $\Delta L_\mathrm{v}^{\mathrm{test}}(f)$ and $\Delta L_\mathrm{v}^{\mathrm{ref}}(f)$ can only be evaluated using the mean vibration velocity levels $\bar{L}_\mathrm{v}(f)$ (as they involve a different set of train passages before and after installation of the barrier).

Figure 9 shows the insertion loss $\mathrm{IL}_z(f)$ at $10\,\mathrm{m}$, $14\,\mathrm{m}$, $18\,\mathrm{m}$, and $32\,\mathrm{m}$ from the track, decomposed according to equations (4) and (5). The interval $\mathrm{IL}_z(f) \pm \sigma_{\mathrm{IL}_z}(f)$ is superimposed in the second case, clearly illustrating the variability of the experimental results. Especially at low frequencies, a large scatter up to $10\,\mathrm{dB}$ and more is observed. At $18\,\mathrm{m}$ and $32\,\mathrm{m}$, the mean and the confidence interval estimates of the insertion loss are consistently above $0\,\mathrm{dB}$ from $8\,\mathrm{Hz}$ upwards. The mean value reaches a maximum of about $10\,\mathrm{dB}$ near $25 - 35\,\mathrm{Hz}$ at $18\,\mathrm{m}$, which is also the frequency range where the highest vibration levels are found during train passages. The insertion loss decreases further away from the barrier at $32\,\mathrm{m}$, although it still reaches almost $7\,\mathrm{dB}$ near $20\,\mathrm{Hz}$ (but vibration levels also decrease further away from the barrier). These results clearly demonstrate the vibration reduction effectiveness of the jet grouting wall. The mean value of the insertion loss remains close to $0\,\mathrm{dB}$ in front of the barrier, except above $30\,\mathrm{Hz}$ at $10\,\mathrm{m}$, where significant negative values are obtained (indicating an amplification). It is emphasized, however, that this results from a reduction of vibration levels at the reference section (for unclear reasons) and not at the test section, which leads to a negative insertion loss through the correction term $\Delta L_\mathrm{v}^{\mathrm{ref}}(f)$ in equation (4). No increase of vibration levels is actually observed at the test section, nor at the reference section (cfr. figure 8a). Figure 9 also illustrates that the correction terms $\Delta L_\mathrm{v}^{\mathrm{ref}}(f)$ in equation (4) are significantly smaller than the correction terms $\Delta L_\mathrm{v}^{\mathrm{before}}(f)$ in equation (5) (except at $10\,\mathrm{m}$), indicating that spatial variations between the reference and test section are more important than variations in time. This suggests that, if no combined procedure can be applied for evaluating the mitigation performance (i.e. if no correction terms can be computed), the methodology corresponding to equation (2) should be favoured over the one corresponding to equation (3).

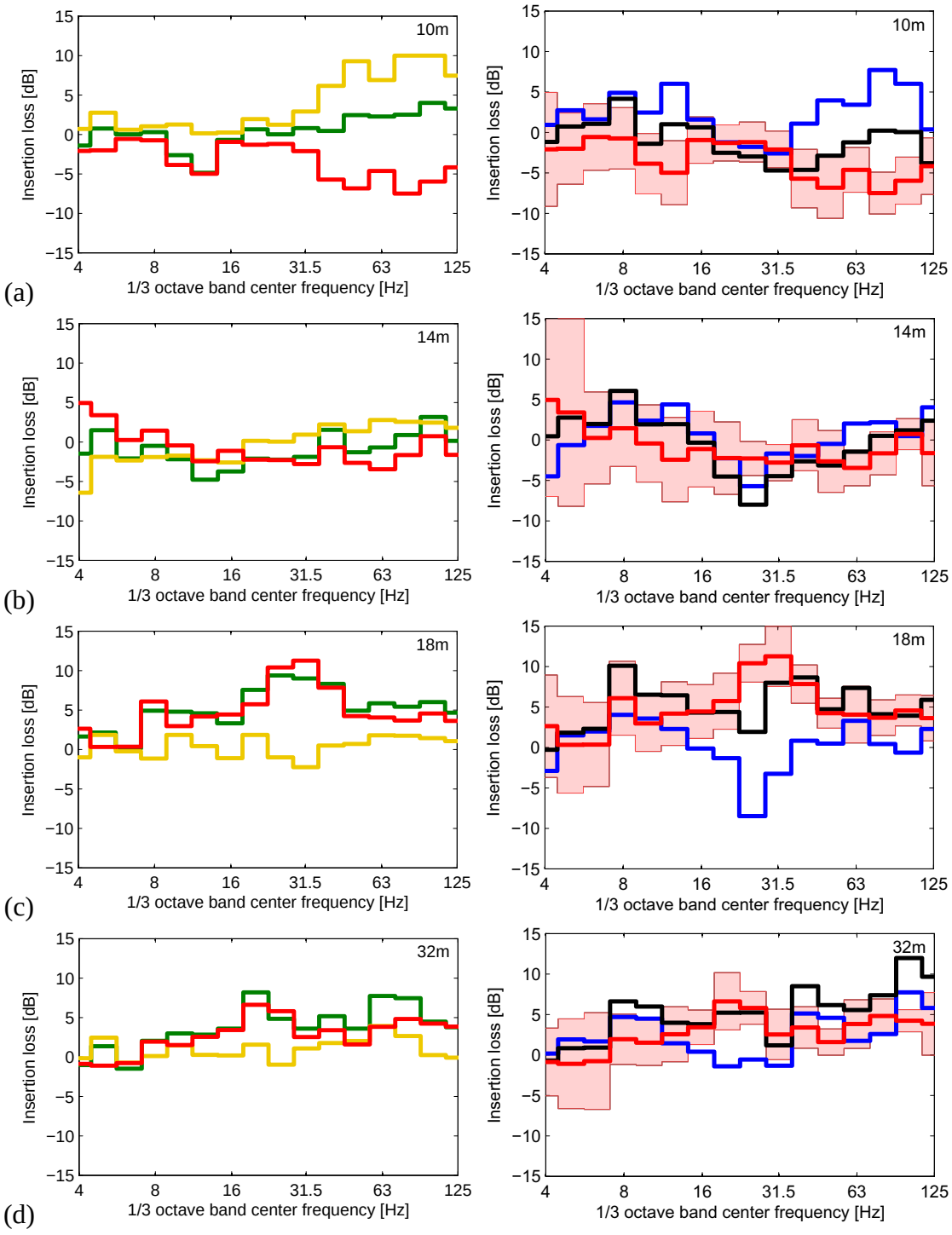

Figure 9: Insertion loss $\mathrm{IL}_z(f)$ in one–third octave bands (red line) during the passage of S592 commuter trains at (a) $10\,\mathrm{m}$, (b) $14\,\mathrm{m}$, (c) $18\,\mathrm{m}$, and (d) $32\,\mathrm{m}$ from the outer rail. The insertion loss is decomposed according to equation (4) (left) into $\Delta L_\mathrm{v}^\mathrm{test}(f)$ (green line) and $\Delta L_\mathrm{v}^\mathrm{ref}(f)$ (yellow line), and according to equation (5) (right) into $\Delta L_\mathrm{v}^\mathrm{after}(f)$ (black line) and $\Delta L_\mathrm{v}^\mathrm{before}(f)$ (blue line). The confidence interval estimates $\mathrm{IL}_z(f) \pm \sigma_{\mathrm{IL}_z}(f)$ of the measurements are indicated as a shaded area for the second decomposition.

The experimental results presented in this subsection clearly demonstrate the effectiveness of the stiff wave barrier for reducing the free field response during train passages. Additional experiments have been performed in order to gain further insight in the dynamic behaviour of the barrier. Furthermore, the measurements have been compared to state-of-the-art numerical simulations; a reasonable agreement was found. The reader is referred to [33] for an elaborate discussion.

4 CONCLUSIONS

In this paper, the experimental and numerical evaluation of the vibration reduction effectiveness of a stiff wave barrier has been discussed. A site with soft soil characteristics was selected at El Realengo and a full scale in situ test was performed. A barrier of $7.5\,\mathrm{m} \times 1\,\mathrm{m} \times 55\,\mathrm{m}$ composed of overlapping jet grout columns was designed and installed near a conventional railway line. Free field vertical vibration velocities were recorded during several train passages at a test and reference section, before and after installation of the barrier. A combined procedure has been adopted for assessing the effectiveness of the jet grouting wall, hence accounting for varying train, track, and soil properties in space and time. The measurements demonstrate that the barrier is very effective, as insertion loss values of $5\,\mathrm{dB}$ are obtained from $8\,\mathrm{Hz}$ upwards, with a peak of almost $12\,\mathrm{dB}$ near $30\,\mathrm{Hz}$, corresponding to the dominant frequency during train passages. The performance decreases further away from the barrier, but remains significant. This in situ test hence serves as a 'proof of concept', demonstrating that stiff wave barriers are capable of significantly reducing vibration levels, provided that they are properly designed.

ACKNOWLEDGEMENTS

The results presented in this paper have been obtained within the frame of the EU FP7 project RIVAS (Railway Induced Vibration Abatement Solutions) [32] under grant agreement No. 265754. The authors would like to thank the project partners involved in the realization of the in situ test at El Realengo (Keller Cimentaciones, ADIF, and CEDEX), and especially Goran Vukotic (Keller Cimentaciones), Álvaro Andrés (ADIF), Miguel Rodríguez (ADIF), and all the members of the geophysical and soil dynamic testing groups of CEDEX's Geotechnical Laboratory.

The first author is a post–doctoral fellow of the Research Foundation Flanders (FWO). The financial support is gratefully acknowledged.

REFERENCES

[1] C.J.C. Jones. Use of numerical models to determine the effectiveness of anti-vibration systems for railways. *Proceedings of the Institution of Civil Engineers-Transport*, 105(1):43–51, 1994.

[2] Y.B. Yang and H.H. Hung. A parametric study of wave barriers for reduction of train-induced vibrations. *International Journal for Numerical Methods in Engineering*, 40(20): 3729–3747, 1997.

[3] A.M. Kaynia, C. Madshus, and P. Zackrisson. Ground vibration from high speed trains: prediction and countermeasure. *Journal of Geotechnical and Geoenvironmental Engineering, Proceedings of the ASCE*, 126(6):531–537, 2000.

[4] G. Lombaert, G. Degrande, B. Vanhauwere, B. Vandeborght, and S. François. The control of ground borne vibrations from railway traffic by means of continuous floating slabs. *Journal of Sound and Vibration*, 297(3-5):946–961, 2006.

[5] H. Loy. Mitigating vibration using under-sleeper pads. *Railway Gazette International*, 168(4):40–43, 2012.

[6] P.A. Costa, R. Calçada, and A.S. Cardoso. Ballast mats for the reduction of railway traffic vibrations. Numerical study. *Soil Dynamics and Earthquake Engineering*, 42:137–150, 2012.

[7] H.H. Hung, Y.B. Yang, and D.W. Chang. Wave barriers for reduction of train-induced vibrations in soils. *Journal of Geotechnical Engineering, Proceedings of the ASCE*, 130(12):1283–1291, 2004.

[8] A. Karlström and A. Boström. Efficiency of trenches along railways for trains moving at sub- or supersonic speeds. *Soil Dynamics and Earthquake Engineering*, 27:625–641, 2007.

[9] S. François, M. Schevenels, B. Thyssen, J. Borgions, and G. Degrande. Design and efficiency of a vibration isolating screen in the soil. *Soil Dynamics and Earthquake Engineering*, 39:113–127, 2012.

[10] D.E. Newland and H.E.M. Hunt. Isolation of buildings from ground vibration: a review of recent progress. *Proceedings of the Institution of Mechanical Engineers, Part C: Journal of Mechanical Engineering Science*, 205:39–52, 1991.

[11] J.P. Talbot and H.E.M. Hunt. A generic model for evaluating the performance of base-isolated buildings. *Journal of Low Frequency Noise, Vibration and Active Control*, 22(3):149–160, 2003.

[12] R.D. Woods. Screening of surface waves in soils. *Journal of the Soil Mechanics and Foundation Division, Proceedings of the ASCE*, 94(SM4):951–979, 1968.

[13] G. Segol, P.C.Y. Lee, and J.F. Abel. Amplitude reduction of surface waves by trenches. *Journal of the Engineering Mechanics Division, Proceedings of the ASCE*, 104(3): 621–641, 1978.

[14] D.E. Beskos, B. Dasgupta, and I.G. Vardoulakis. Vibration isolation using open or filled trenches. Part I: 2-D homogeneous soil. *Computational Mechanics*, 1: 43–63, 1986.

[15] R. Klein, H. Antes, and D. Le Houédec. Efficient 3D modelling of vibration isolation by open trenches. *Computers and Structures*, 64:809–817, 1997.

[16] M. Kim, P. Lee, D. Kim, and H. Kwon. Vibration isolation using flexible rubber chip barriers. In G. Schmid and N. Chouw, editors, *Proceedings of the International Workshop Wave 2000, Wave propagation, Moving load, Vibration reduction*, pages 289–298. A.A Balkema, Amsterdam, 2000.

[17] A. Alzawi and M.H. El Naggar. Full scale experimental study on vibration scattering using open and in-filled (geofoam) wave barriers. *Soil Dynamics and Earthquake Engineering*, 31(3):306–317, 2011.

[18] P.K. Banerjee, S. Ahmad, and K. Chen. Advanced application of BEM to wave barriers in multi-layered three-dimensional soil media. *Earthquake Engineering and Structural Dynamics*, 16: 1041–1060, 1988.

[19] L. Andersen and S.R.K. Nielsen. Reduction of ground vibration by means of barriers or soil improvement along a railway track. *Soil Dynamics and Earthquake Engineering*, 25:701–716, 2005.

[20] X. Sheng, C.J.C. Jones, and D.J. Thompson. Modelling ground vibrations from railways using wavenumber finite- and boundary-element methods. *Proceedings of the Royal Society A - Mathematical, Physical and Engineering Sciences*, 461:2043–2070, 2005.

[21] S.E. Kattis, D. Polyzos, and D.E. Beskos. Vibration isolation by a row of piles using a 3-D frequency domain BEM. *International Journal for Numerical Methods in Engineering*, 46:713–728, 1999.

[22] V.V. Krylov. Scattering of Rayleigh waves by heavy masses as method of protection against traffic-induced ground vibrations. In H. Takemiya, editor, *Environmental vibrations. Prediction, Monitoring, Mitigation and Evaluation*, pages 393–398. Taylor and Francis Group, London, 2005.

[23] A. Dijckmans, P. Coulier, J. Jiang, M.G.R. Toward, D.J. Thompson, G. Degrande, and G. Lombaert. Mitigation of railway induced vibrations by using heavy masses next to the track. In A. Cunha, E. Caetano, P. Ribeiro, and G. Müller, editors, *Proceedings of the 9th International Conference On Structural Dynamics, EURODYN 2014*, pages 751–758, Porto, Portugal, 2014.

[24] T.M. Al-Hussaini, S. Ahmad, and J.M. Baker. Numerical and experimental studies on vibration screening by open and in-filled trench barriers. In G. Schmid and N. Chouw, editors, *Proceedings of the International Workshop Wave 2000, Wave propagation, Moving load, Vibration reduction*, pages 241–250. A.A Balkema, Amsterdam, 2000.

[25] E. Celebi, S. Firat, G. Beyhan, I. Cankaya, I. Vural, and O. Kirtel. Field experiments on wave propagation and vibration isolation by using wave barriers. *Soil Dynamics and Earthquake Engineering*, 29(5):824–833, 2009.

[26] F. De Cock and C. Legrand. Influence of underground gas cushions on the wave propagation of ground vibrations. In *Proceedings of the 4th International Conference on the Application of Stress Wave Theory to Piles*, The Hague, The Netherlands, September 1992.

[27] K.R. Massarsch. Vibration isolation using gas-filled cushions. In *Proceedings of the Geo-Frontiers 2005 Congress*, Austin, Texas, January 2005. American Society of Civil Engineers.

[28] W. Haupt. Model tests on screening of surface waves. In *Proceedings of the 10th International Conference on Soil Mechanics and Foundation Engineering*, volume 3, pages 215–222, 1981.

[29] C. Murillo, L. Thorel, and B. Caicedo. Ground vibration isolation with geofoam barriers: Centrifuge modeling. *Geotextiles and Geomembranes*, 27(6):423–434, 2009.

[30] P. Coulier and H.E.M. Hunt. Experimental study of a stiff wave barrier in gelatine. *Soil Dynamics and Earthquake Engineering*, 66:459–463, 2014.

[31] P. Coulier, S. François, G. Degrande, and G. Lombaert. Subgrade stiffening next to the track as a wave impeding barrier for railway induced vibrations. *Soil Dynamics and Earthquake Engineering*, 48:119–131, 2013.

[32] http://www.rivas-project.eu, 2011.

[33] P. Coulier, V. Cuéllar, G. Degrande, and G. Lombaert. Experimental and numerical evaluation of the effectiveness of a stiff wave barrier in the soil. *Soil Dynamics and Earthquake Engineering*, Accepted with minor revisions.

[34] D.J. Ewins. *Modal testing: theory and practice*. Research Studies Press Ltd., Letchworth, UK, 1984.

[35] P. Coulier, A. Dijckmans, S. François, G. Degrande, and G. Lombaert. A spatial windowing technique to account for finite dimensions in 2.5D dynamic soil–structure interaction problems. *Soil Dynamics and Earthquake Engineering*, 59:51–67, 2014.

[36] A.C. Eringen and E.S. Suhubi. *Elastodynamics, Volume 2, Linear theory*. Academic Press, New York, USA, 1975.

[37] International Organization for Standardization. *ISO 2631-2:1997: Mechanical vibration and shock - Evaluation of human exposure to whole-body vibration - Part 1: General requirements. Second Edition*, 1997.

[38] Deutsches Institut für Normung. *DIN 45672 Teil 2: Schwingungsmessungen in der Umgebung von Schienenverkehrswegen: Auswerteverfahren*, 1995.

[39] D. Stiebel. Protocol for free field measurements of mitigation effects in the project RIVAS for WP 2, 3, 4, 5. RIVAS project SCP0-GA-2010-265754, Deliverable D1.2, Report to the EC, October 2011.